Colloids in Optical Fields

Gabriel C. Spalding[1], Onofrio M. Maragò[2], and Giovanni Volpe[3,4]

1. Introduction

2. Brief History of Optical Manipulation

3. Fundamentals

- **a. Scattering forces and the counter-propagating trap**
- **b. Gradient forces and the optical tweezers**
- **c. Optical binding**

4. Single colloids: *The bead, the spring and the fluid.*

- **a. Brownian motion and the Langevin equation**
- **b. Brownian motion in a harmonic trap**
- **c. Measuring and exerting forces**
- **d. Metallic particles and localized surface plasmons**
- **e. Low dimensional nanostructures**
- **f. Optical trapping in vacuum**

5. Many-particle systems and extended light fields: *The power of many.*

- **a. Optical ratchets and sorting in optical lattices**
- **b. Optical crystallization and melting**
- **c. Optical crystals and quasi-crystals**

6. Advanced techniques: *One beam to rule them all.*

- **a. Holographic optical tweezers**
- **b. Beams with orbital angular momentum**
- **c. Applications to microfluidics**

7. Bibliography

[1] Department of Physics, Illinois Wesleyan University, Bloomington, IL 61701, USA.

Email:gspaldin@iwu.edu

[2] CNR-IPCF, Istituto per i Processi Chimico-Fisici, V.le F. Stagno D'Alcontres, 37, I-98158 Messina, Italy.
Email: marago@me.cnr.it

[3] Physikalisches Institut, Universität Stuttgart, Pfaffenwaldring 57, D-70550 Stuttgart, Germany.

Email: g.volpe@physik.uni-stuttgart.de

[4] Max-Planck-Institut für Intelligente Systeme, Heisenbergstraße 3, D-70569 Stuttgart, Germany.

1. Introduction

It is well known from quantum mechanics that light carries momentum: for a photon at wavelength λ the associated momentum is $p = h/\lambda$, where h is Planck's constant. For this reason, whenever an atom emits or absorbs a photon, its momentum changes according to Newton's laws. Similarly, an object will experience a force whenever a propagating light beam is absorbed, refracted or reflected by its surface. In most situations optical forces are so much smaller than other forces acting on macroscopic objects that there is no noticeable effect and, therefore, can be neglected. However, the experiments we consider involve objects that weigh less than 1 μg, with a size less than tens of micrometers; here, the radiation pressure exerted by light becomes an exquisite tool. Fig. 1 presents a variety of objects that are commonly manipulated using optical fields; among these, colloidal particles feature prominently.

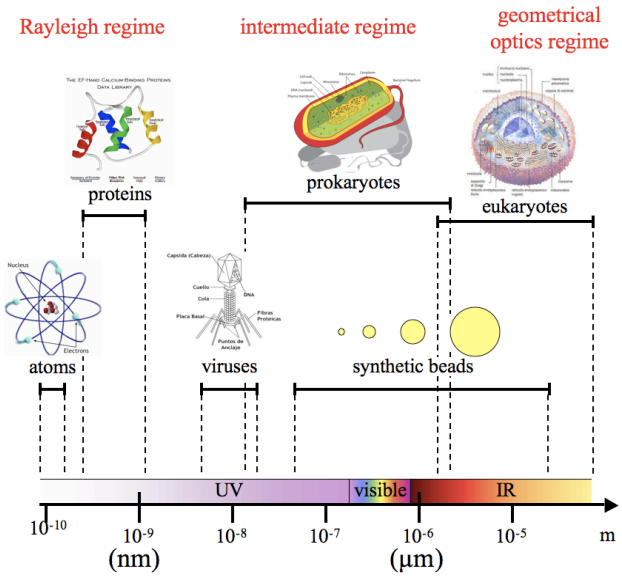

Figure 1. Typical objects that are manipulated using optical fields and corresponding trapping regimes.

In 1970 a seminal paper by Arthur Ashkin showed that it was possible to use radiation forces to significantly affect the dynamics of a colloidal particle. In 1986, Ashkin and colleagues reported the first observation of what is now commonly referred to as *optical tweezers*: a tightly focused light beam capable of holding colloidal particles in three dimensions. Since then, a wide variety of tailored optical fields have been used to study a wide range of colloidal materials under a wide spectrum of conditions. For example, beyond trapping a single particle, tailored light beams have been used to trap multiple colloids at the same time and to provide complex potential landscapes permitting scientists to study the behavior of large ensembles of colloidal particles. The interplay between deterministic optical forces and the random Brownian fluctuations has been established as a valuable tool for studying fundamental phenomena in statistical physics. At base level, optically trapped colloids have been used as very sensitive force probes capable of measuring tiny forces and even torques, and optical traps provide for precise positioning and for dexterous control of small components.

2. Brief History of Optical Manipulation

The ability of light to exert forces was, at least tentatively, recognized as far back as 1619 when Kepler described in his book, *De Cometis,* the deflection of comet tails by the sun. In the late XIX century Maxwell's theory of electromagnetism quantitatively calculated the *momentum flux* in a light beam, showing it to be proportional to the intensity and predicting that optical momentum could be transferred to illuminated objects,

resulting in a *radiation pressure* pushing objects along the direction of propagation (see Fig. 2). Exciting early experiments were performed that detected these effects. At the start of the twentieth century, Nichols and Hull and, independently, Lebedev first succeeded in detecting the small effect of radiation pressure upon macroscopic objects and absorbing gases. A few decades later in 1936 Beth reported the first experimental observation of the torque on a macroscopic object resulting from interaction with light: he observed the deflection of a quartz wave plate suspended from a thin quartz fiber when circularly polarized light passed through it. As these initial experiments involved macroscopic objects, the effects were *not* easily detected. Quoting J. H. Poynting's presidential address to the British Physical Society in 1905, "a very short experience in attempting to measure these forces is sufficient to make one realize their extreme minuteness – a minuteness which appears to put them beyond consideration in terrestrial affairs."

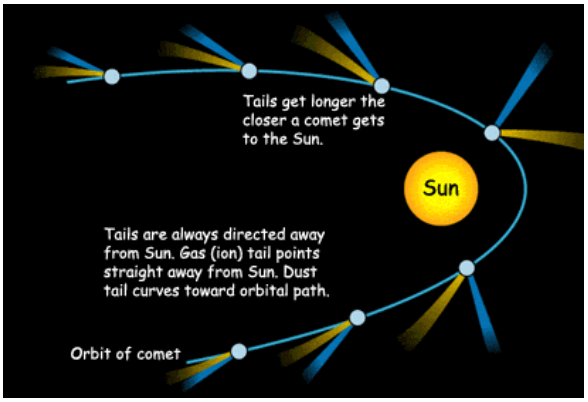

Figure 2. Deflection of comet tails by the scattering force of the light coming from the Sun. [from NASA]

This situation changed significantly after the invention of the laser in the 1960s. In 1970 the seminal paper from Ashkin showed that it was possible to use the forces of radiation pressure to significantly affect the dynamics of transparent *micrometer-sized* neutral particles. Two basic light pressure forces were identified: a ***scattering force*** in the direction of the incident beam and a ***gradient force*** in the direction of the intensity gradient of the beam. It was shown experimentally that, using just these forces, one could accelerate, decelerate, and even stably trap small micrometer-sized neutral particle using focused laser beams.

Ashkin started by considering a beam of power P reflecting on a plane mirror. In this case there are $P/h\nu$ photons per second striking the mirror and each of them carries a momentum $h\nu/c$. If all of them are reflected straight back, the total change in light momentum per second is $2\cdot(P/h\nu)\cdot(h\nu/c)=2P/c$, which, by conservation of momentum, implies that the mirror experiences an equal and opposite force in the direction of the light. This is the maximum force that one can extract form the light. Quoting Ashkin [Ashkin (2000)], "Suppose we have a laser and we focus our one watt to a small spot size of about a wavelength ~1μm, and let it hit a particle of diameter also of 1 μm. Treating the particle as a 100%-reflecting mirror of density ~1gm/cm^3, we get an acceleration of the small particle, $a = F/m = 10^{-3}$ dynes/10^{-12} gm = 10^9 cm/sec^2. Thus, a~$10^6 g$, where g~10^3cm/sec^2 is the acceleration of gravity. This a is quite large and should give readily observable effects, so I tried a simple experiment. [...] It is surprising that this simple first experiment [...], intended only to show forward motion due to laser radiation pressure, ended up demonstrating not only this force but the existence of the transverse force component, particle guiding, particle separation, and stable 3D particle trapping."

In 1986, Ashkin and colleagues reported the first observation of what is now commonly referred to as an optical trap: a tightly focused beam of light capable of holding microscopic particles in three dimensions. One of Ashkin's co-authors, Steven Chu, would go on to use optical forces in his work on cooling and trapping atoms. This research earned Chu, together with Claude Cohen-Tannoudji and William Daniel Phillips, the 1997 Nobel Prize in Physics.

In the late 1980s, Arthur Ashkin and his colleagues applied the new technology to the biological sciences, starting by trapping an individual tobacco mosaic virus and Escherichia coli bacterium (E-coli). In the early 1990s, Steven Block, Carlos Bustamante, and James Spudich pioneered the use of optical trap force spectroscopy to characterize the mechanical properties of biomolecules and biological motors. These molecular motors are ubiquitous in biology, and are responsible for locomotion and mechanical action within the cell. Optical traps allowed these biophysicists to observe the forces and dynamics of nanoscale motors at the single-molecule level. Optical trap force-spectroscopy has led to greater understanding of the nature of these force-generating molecules. Optical tweezers have also proven useful in many other areas of physics, such as atom trapping and statistical physics.

3. Fundamentals

In optical trapping experiments, the light force is provided by a laser beam and objects ranging from tens of nanometers to tens of micrometers, such as cells, micron-sized dielectric particles or nano-sized metallic beads, linear nanostructures, are manipulated. Considering the ratio between the characteristic dimension L of the object and the wavelength λ of the trapping light, three different trapping regimes can be defined:

1. *Rayleigh regime*, when $L << \lambda$;

2. *Intermediate regime*, when L is comparable to λ;

3. *Geometrical optics regime*, when $L >> \lambda$.

Figure 1 shows typical objects that belong to each of these regimes.

In any of these regimes, the electromagnetic equations can in principle be solved to evaluate the force acting on the object. However, this can be a cumbersome task. For the Rayleigh regime and geometrical optics regime approximated models have been developed, which allow one to gain insights into the physics of optical trapping. Indeed most of the objects that are normally trapped in optical manipulation experiments fall in the intermediate regime region, where the Rayleigh or geometrical optics approximation cannot be used. Thus whenever a quantitative comparison between theory and experiments is sought, the full electromagnetic theory has to be used for the calculations of optical forces.

Even though optical forces have a common origin in the interaction between light and matter and can be inferred from the solution of the corresponding electromagnetic equations, they have been schematically classified in three main kinds, corresponding to *scattering forces*, *gradient forces*, and *optical binding forces*.

3.a. Scattering forces and the counter-propagating trap

The *scattering force* was the first one to be identified. This force is proportional to the light intensity and always points in the direction of the incident light and. Therefore it cannot be used directly to generate a stable trap. As Ashkin reports [Ashkin (2000)], "I used a sample of transparent latex spheres of density ~1 [g/cm^3], in water, to avoid any problems with heating or so-called radiometric effects. With just milliwatts of power, particle motion was observed in the direction of a mildly focused Gaussian beam. The particle velocity was in approximate agreement with our crude-force estimates, suggesting that this was indeed a radiation pressure effect."

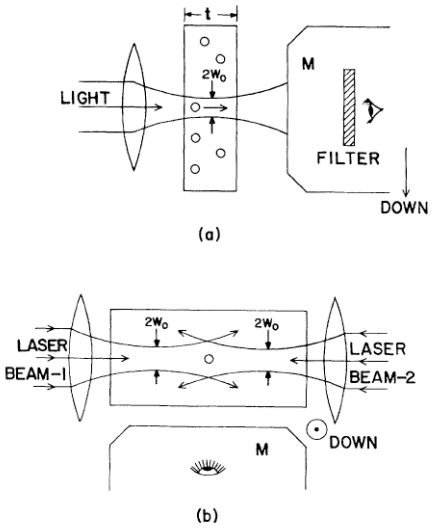

Figure 3. (a) The scattering optical force pushes colloidal particles in the direction of the incident beam. (b) Two counter-propagating beams can stably trap a colloid in three dimensions. [from Ashkin (1970)].

In 1970 Ashkin [Ashkin (1970)] proposed a configuration where two counter-propagating beams could stably trap a particle, as shown in Fig. 3, and later reported some experiments where the scattering force was levitating a particle against gravity [Ashkin and Dziedzic (1971)].

3.b. Gradient forces and the optical tweezers

In 1986 Ashkin and coworkers demonstrated that it is indeed sufficient a single highly focused laser beam in order to trap a colloidal particle in three dimensions. This is thanks to the so-called *gradient force*, which was also initially identified by Ashkin (1970). This force arises from the presence of a gradient in the intensity of an optical field and tends to attract particles with refractive index higher than their surrounding towards the high-intensity regions of the field (*high-field seekers*), and conversely particles with lower refractive index towards the low-intensity regions (*low-field seekers*). This is what is now referred to as *optical tweezers* [Ashkin *et al*. (1986)].

Using simple ray diagrams it is possible to provide a very detailed picture of the physics of the trapping process, without the need for the use of involved calculus and electromagnetic theory. As can be appreciated from the Fig. 4(a), when a light ray enters a transparent dielectric sphere it undergoes deflection as a result of refraction at the interfaces. Such deflection of photons that carry momentum results in a recoil force. This force [dark gray arrow in Fig. 4(a)] however does not trap the particle; it only pushes the sphere away from the light. To trap an object it is necessary to use a set of light-rays coming from different directions. If two light-rays come from opposite sides of the dielectric sphere at a very high angle they can indeed trap the particle [Fig. 4(b)]. It can be easily appreciated from similar ray diagrams what happens when the sphere is displaced both axially [Fig. 1(c)] and laterally [Fig. 4(d)] with respect to the focus. In this cases the total force (black arrow) pushes the particle towards the optical trap center arises.

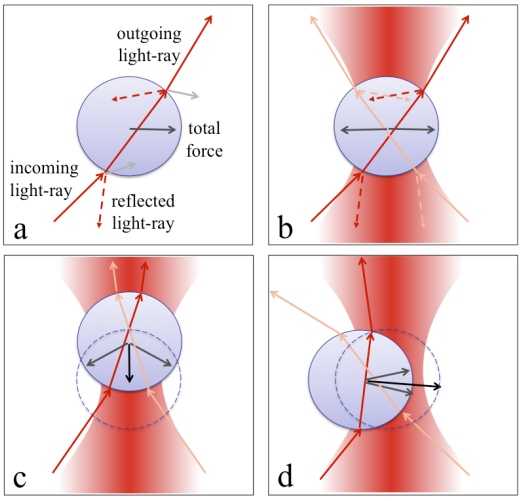

Figure 4. Optical forces on a dielectric sphere as they can be understood with a ray diagram. (a) A light-ray (red) exert a force (dark gray) arising from its refraction and reflection. (b) The forces (dark gray) due to two light-rays (red and orange) acting on a sphere compensate each other at the equilibrium position. (c) Restoring force on a axially displaced sphere. (d) Restoring force on a laterally displaced sphere.

A simple example is a highly focused laser beam. This acts as an attractive potential well for a particle. The equilibrium position lies near – but not exactly at – the focus. When the object is displaced form this equilibrium position, it experiences an attractive force towards it. This restoring force is in first approximation proportional to the displacement; in other words, the optical tweezers' force can generally be described by Hooke's law:

$$F_x = -k_x (x - x_0), \qquad (3.b.1)$$

where x is the particle's position, x_0 is the focus position, and k_x is the optical trap spring constant along x, usually referred as trap stiffness. In fact, optical tweezers create a tridimensional potential well that can be approximated by three independent harmonic oscillators, one for each of the x, y, and z directions. In the xy-plane (perpendicular to the direction of the beam propagation) the force is mainly due to gradient optical forces, while along the z-direction (along the direction of the beam propagation) the restoring gradient force is weakened by the presence of the scattering force.

More complex intensity patterns have been obtained, for example, by interfering two or more light beams or by the use of advanced techniques such as holography and time multiplexing.

3.c. Optical binding

Optical binding forces arise in the presence of multiple particles. These particles may scatter the incoming light and the scattered light may induce optical forces on the nearby particles. Such forces can bind together many particles, therefore their name, generating what is know as *optical matter*. The existence of optical binding forces was recognized only much later than scattering and gradient forces [Burns *et al*. (1989)].

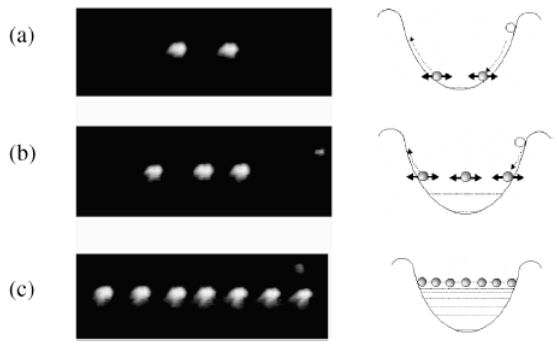

Figure 5. Experimental data for arrays of (a) two, (b) three, and (c) seven spheres (each 3 mm in size). The diagrams on the right elucidate how we fill up the approximately harmonic potential well created by the two counter-propagating beams and how optical binding forces (represented by the arrows) keep the particles apart from each other. [from Tatarkova (2002)]

4. Single colloids: *The bead, the spring and the fluid.*

As we will see in this section, the behavior of a colloidal particle trapped by an optical tweezers is exquisitely sensitive to its environment. As a prequel, consider Fig. 6, which shows both that the trajectories of trapped particles are stochastic in nature, and that the degree confinement within the trap increases as a function of the laser power [Volpe *et al*. (2009)].

In 1993 Ghislain and coworkers devised a new kind of scanning force microscopy using such an optically trapped microsphere as a probe [Ghislain and Webb (1993); Ghislain *et al*. (1994)], later called the *Photonic Force Microscope* (PFM) [Florin *et al.* (1998)]. The PFM provides the capability of measuring forces in the range from femtonewtons to piconewtons. Such values are well below what can is achieved with alternative techniques based on microfabricated mechanical cantilevers, *e.g*. atomic force microscopy [Binnig *et al*. (1986)].

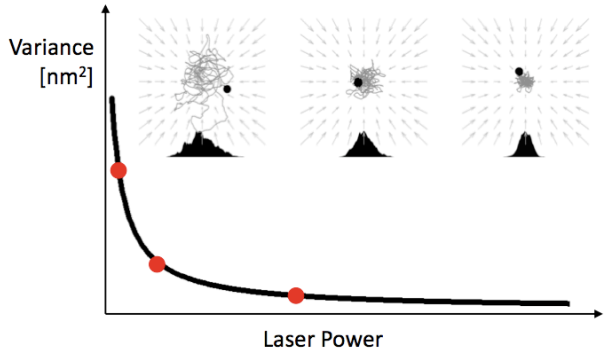

Figure 6. Brownian trajectories in the *xy*-plane of an optically trapped particle as a function of the trapping laser power.

4.a. Brownian motion and the Langevin equation

The motion of colloidal particles suspended in a fluid was first described in details by botanist Robert Brown in the late eighteenth century while observing plant pollen and sphinx dust under a microscope [Brown (1828)]. This motion goes now by the name of *Brownian motion* and its mathematical description has become an

essential tool throughout physical, chemical, biological sciences, and even finance [Nelson (1967)]. Historically this mysterious random movement was ascribed to thermal agitation from the surrounding molecules [Gouy (1888)], leading to Einstein's famous predictions, during his *annus mirabilis* [Einstein (1905)], regarding particle diffusion. In brief, Einstein considered the random walk of the colloidal particle in a fluid, and showed that the mean square of the particle displacement, $x(t)$, increases linearly with time, *i.e.* $\langle x^2(t)\rangle \propto t$. As shown below, the constant of proportionality is typically written as $\langle x^2(t)\rangle = 2Dt$, where D is the particle diffusion constant, which is related to the temperature of the fluidic environment, and the degree of hydrodynamic drag via the Einstein-Stokes relation:

$$D_{SE} = \frac{k_B T}{6\pi\eta a} \tag{4.a.1}$$

The denominator reflects the amount hydrodynamic drag expected from Stokes' law, which states that, in a fluid with dynamical viscosity η, a spherical colloid of radius a moving at low speeds, far from other particles or surfaces, will experience a drag force $f_{\text{drag}} = -(6\pi\eta a)v$.

Einstein's results are simplest to explore using a different approach than the one he originally used. It is now most common to invoke a stochastic differential equation known as the *Langevin equation*, developed by Langevin in 1908, based on a decomposition of the total force acting on the particle into two separate terms – an average component describing the hydrodynamic drag, and a fluctuating component $f(t)$ with $\langle f(t)\rangle = 0$ [Langevin (1908)]. For a *free* (un-trapped) Brownian particle of mass m the dynamics are described by the following Langevin equation:

$$m\frac{d^2x}{dt^2} = -\gamma\frac{dx}{dt} + f(t) \tag{4.a.2}$$

This dynamical equation can be solved by considering the time-averaged variables. Assuming that the particle displacement is statistically independent (uncorrelated) of the fluctuating force, *i.e.* $\langle xf\rangle = 0$, and that the particle is in thermal equilibrium with the surrounding fluid is possible to show that [see, *e.g.*, Pecseli (2000)]:

$$\frac{d\langle x^2\rangle}{dt} = 2D\left[1 - e^{-\gamma t/m}\right] \tag{4.a.3}$$

Thus at extremely short times the particle follows a ballistic regime (root-mean square displacement is linear with time) while at longer times the diffusive regime is recovered (mean square displacement is linear with time). The cross-over between these two regimes, which was predicted more than a century ago, has been elusive for many years and has only recently been observed [Li *et al*. (2010); Huang *et al*. (2011)] using optically trapped particles (see Fig. 7). Note how the particle diffusion is independent of its mass. This only enters in the exponential term of Eq. 4.a.3 and thus for large particles the mass term in the Langevin equation is negligible.

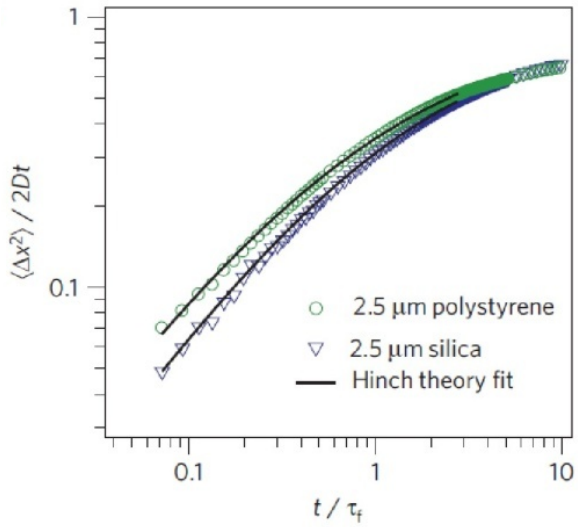

Figure 7. Transition from ballistic (slope = 2) to diffusive (slope = 1) for the mean square displacement (MSD) for 2.5 µm silica and polystyrene particles. The timescale is normalized to the crossover time τ_f, and the MSD is normalized to the value in the free-diffusion regime $2Dt$. Note that τ_f is the same for both particles. (Reprinted from [Huang *et al*. (2011)]).

4.b Brownian motion in a harmonic trap

When a Brownian particle is subject to an external field, *e.g*. a confining potential, a special class of solutions to the dynamics of its motion occurs, originally studied by Uhlenbeck and Ornstein (1930). The fluid damps the colloidal particle motion as in the free-diffusive case, but now the confining potential acts as a cut-off to the particle displacement, *i.e*., the particle explores only a limited region in space. This means that the particle motion has a free diffusive character for short times (high frequency limit), while is frozen at longer times (low frequency limit). These Ornstein-Uhlenbeck processes have perfect ground in experiments with optical traps, where a colloidal particle is held by an optical tweezers. In this context, Brownian motion can be utilized to investigate the properties of the surrounding environment, *i.e*., for microrheology investigations, as well as of the trapped particle, and for accurate calibration of the spring constants of the optical harmonic potential [Rohrbach (2005); Seol (2006)]. Indeed Brownian motion is the crucial element in force sensing applications with optical tweezers [Florin (1998); Pralle (1999)]. In experiments with optically trapped particles, position fluctuations are tracked by position sensing detectors, *e.g*., quadrant photodiodes (QPD). Thus the particle positional fluctuations appear as randomly fluctuating signal voltages, similar to those shown in the traces of Fig. 5(a). The statistical analysis of these fluctuations enables force calibration and measurements [Florin (1998); Berg-Sørensen (2004); Meiners (1999); Henderson (2001); Martin (2005) MORE REFS]

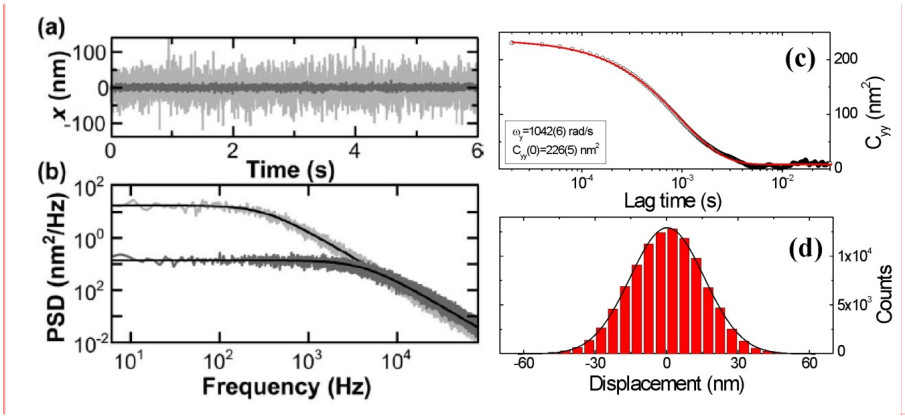

Figure 8. Calibration of optical tweezers. (a) Position record of a 100-nm gold (dark gray) and a 110-nm polystyrene (light gray) bead. (b) Averaged power spectra fit for the same gold (dark gray) and polystyrene bead (light gray). Lorentzian fits (solid curve) yield relaxation frequencies and eventually force sensing calibration {(a) and (b) from [Seol *et al*. (2006)]}. (c) Histogram of the random displacements and (d) autocorrelation analysis for an optically trapped 2-μm latex bead.

Gabriel Spalding 4/8/13 2:15 PM
Comment [1]: The left-axis scale on (b) is messed up, going from 10^-2 to 10^2 then back down to 10^0 and back up to 10^2. Also, it would be nice to have consistent notation for the PSD which, in the current body of the manuscript, we tend to call S(f).

4.c. Measuring and exerting forces

The starting point for optical tweezers calibration based on Brownian motion analysis is the Langevin equation in a confining harmonic potential $V(x) = \Sigma \frac{1}{2} k_i x_i^2$. For a trapped spherical particle of size a the generalization of Eq. 4.a.2 (neglecting the mass term) can be written as:

$$\frac{d}{dt} x_i(t) = -\omega_i x_i(t) + \xi_i(t), \qquad i = x,y,z \tag{4.c.1}$$

Where the relaxation frequency $\omega_i = k_i / \gamma$ are proportional to the force constants k_i of the optical trap and the terms $\xi_i(t) = f_i(t) / \gamma$ describe the random fluctuations of the force. This has zero mean, $\langle \xi_i(t) \rangle = 0$, and delta-like correlations, $\langle \xi_i(t) \xi_j(t+\tau) \rangle = 2D \cdot \delta(\tau) \delta_{ij}$, typical of an ideal white noise power spectrum, $\left| \tilde{\xi}_i(\omega) \right|^2 = \langle \xi_i^2(t) \rangle = 2D$.

In order to get the force constants from experimental particle tracking signals, two major procedures are used that rely on a frequency domain (*power spectrum density*) and time domain (*autocorrelation function*) analysis of the thermal fluctuations in the trap. In the first we consider the Fourier transform of Eq. (4.c.1):

$$-i\omega \tilde{x}_i(\omega) = -\omega_i \tilde{x}_i(\omega) + \tilde{\xi}_i(\omega) \tag{4.c.2}$$

and solve for:

$$\tilde{x}_i(\omega) = \frac{\tilde{\xi}_i(\omega)}{-i\omega + \omega_i} \tag{4.c.3}$$

Thus, because of the random force white noise power spectrum, the corresponding power spectral density of the positional fluctuations has a Lorentzian shape:

$$S(\omega) = \left|\tilde{x}_i(\omega)\right|^2 = \frac{2D}{\omega^2 + \omega_i^2} \tag{4.c.4}$$

with a half-width ω_i and a zero frequency point value 2*D* related to the force constants and thermal diffusion respectively.

In the time domain it is instead useful to consider the autocorrelation functions of the position fluctuations:

$$C_{ii}(\tau) = \left\langle x_i(t)\, x_i(t+\tau) \right\rangle \tag{4.c.5}$$

That from Eq. (4.c.1) obey first order uncoupled differential equations with the lag time τ:

$$\frac{d}{d\tau} C_{ii}(\tau) = -\omega_i C_{ii}(\tau) \tag{4.c.6}$$

Equation (4.c.6) can be easily integrated, giving exponential decays, $C_{ii}(\tau) = C_{ii}(0) \cdot e^{-\omega_i \tau}$, with relaxation frequencies ω_i and zero point value $C_{ii}(0) = D / \omega_i$. Examples of these procedures are shown in Fig. 6. In Fig. 6(a) the tracking signals for a gold nanoparticle (dark gray trace) and a polystyrene bead (light gray) are compared, while their power spectra are shown in Fig. 6(b). The Lorentzian curve fitting of these spectra yields the force constants and a full calibration of the optical trap. In Fig. 6(c) we show a typical autocorrelation function of a tracking signal for a 2-mm latex bead. In this case, *i.e.* in the time domain, the force constants and the calibration of the optical tweezers can be obtained by fitting the autocorrelation function with an exponential decay. After calibration is achieved, a reconstruction of the random displacements in the trap is also obtained, as shown in Fig. 6d. As anticipated the motion is confined within the trap region and by fitting the displacement with a Gaussian, typical root-mean square displacements in the nanometer range are obtained. The statistical analysis of the Brownian motion in the trap can be also visualized in three-dimensions by plotting the reconstructed trajectories of the trapped particles. In Fig. 8, the evolution of the trajectories for a spherical particle (top) and a highly anisotropic nanotube bundle (bottom) are compared, showing how both particles explore with time the trapping region.

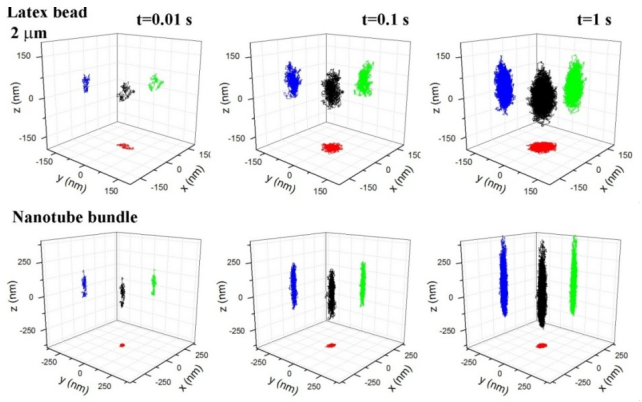

Figure 9. Reconstruction of Brownian motion at different times for a 2-μm latex bead (top) and a nanotube bundle (bottom) in the calibrated optical trap. Note the change of scale between top and bottom plots (data redrawn from [Maragò *et al*. (2008)]).

In both frequency- or time-domain analysis, obtaining the two fitting parameters enables measurements of displacements with nanometric precision, and force sensing with sub-piconewton precision. The capabilities of such highly sensitive force transducers have been exploited in a wealth of experiments at the molecular scale opening a new paradigm in biophotonics. A milestone experiment is described in Fig. 9. Ultra-stable optical trapping with Angstrom-level resolution enabled to study DNA transcription by RNA polymerase (RNAP) with sufficient resolution to observe base pair stepping and error correction directly [Abbondanzieri *et al*. (2005)]. During the transcription process RNAP moves processively along a DNA template, creating a complementary RNA. These experiments demonstrated that the step size of RNAP is equivalent to the distance of a single pair base, of the order of 3.7±0.6 Å, and revealed key details involved in error correction during the transcription process. Moreover the force exerted by RNAP during transcription was measured to be of the order of 14 pN.

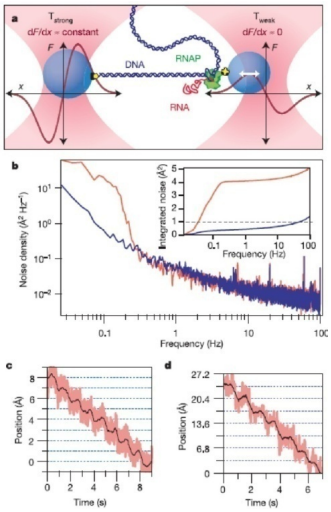

Figure 10. Force measurements during DNA transcription. (a) A highly sensitive double optical tweezers is used to trap two latex beads. One is held in a strong optical trap (left) and is bound to a DNA molecule, the second one is held in a weak trap and coupled to RNAP. During transcription, as RNAP extends along the DNA, displacement and force are measured. (b)

Power spectrum acquired for a stiffly trapped bead with external optics under air (red) or helium (blue). The noise reduction (inset) was a crucial element of the experiment. (c) Steps resolved for a stiffly held bead moved in 1-Å increments at 1 Hz. (d) Steps resolved for a bead-DNA-bead dumbbell held at 27 pN of tension and moved at 3.4-Å steps. (Reprinted from ref. [Abbondanzieri *et al*. (2005)]).

4.d. Metallic particles and localized surface plasmons

A special class of colloids are noble metal nanoparticles (MNP). They have outstanding optical properties that led to a growing interest for applications in physics, chemistry, material and life sciences [REFS]. Their ability to enhance and focus optical fields to spots much smaller than the diffraction limit stems from the occurrence of *localized surface plasmons* (LSPs), *i.e.*, collective wave-like motion of free electrons on the particle surface. All their optical properties, *e.g.* dielectric constants, polarizability, extinction cross-sections, are dictated by such plasmon resonances [REFS] (see Fig.10). LSPs yield a local field-enhancement that can be as large as three orders of magnitude with respect to dielectric particles. In particular, gold and silver nanoparticles are chemically stable and typically exhibit LSPs in the visible wavelength range. Field-enhancement can be very large even in the near-infrared spectral region by changing size, shape and materials. Consequently, the occurrence of LSPs also yields an increase in the optical forces on MNPs when compared with the optical forces on a dielectric particle, resulting in the stabilization of their optical trapping against the increased Brownian motion related to their small size. For gold spherical particles a ten-fold enhancement in optical forces compared to forces on dielectric spheres at 1064nm trapping wavelength has been calculated [Saija (2009)] and measured [Hansen (2005), Seol (2006), Bosanac (2008)]. The smallest particle to date held in an optical tweezers is a 9-nm diameter gold nanosphere [Hajizadeh (2010)].

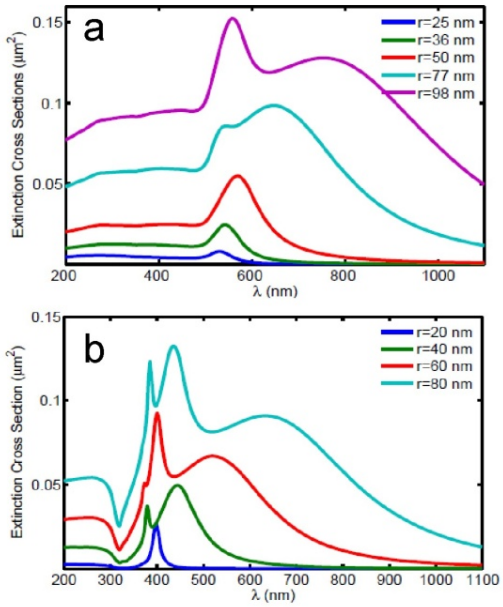

Figure 11. Calculated extinction cross-section for gold (a) and silver (b) nanospheres of different radii. For the larger particles higher-order plasmonic modes occur. The refractive index that has been used is the one tabulated by Johnson and Christy [REF]. (Redrawn from [Saija *et al*., (2009)].

Optical tweezers have been used to hold and manipulate individual metal nanoparticles since the pioneering work of Svoboda and Block [Svoboda (1998)]. Plasmon-enhanced optical trapping has been demonstrated on a large variety of metal colloids. Bi-pyramids and nanorods have been trapped and manipulated […]. Both

trapping and repulsive optical forces have been shown to operate on metal spherical nanoparticles depending on size […..] and wavelength […] demonstrating the crucial role of the plasmon resonance. In fact, since the gradient force is related to the real part of the particle polarizability, in the case of a resonant system, such as an MNP, this has a dispersive character. Thus the trapping force on MNPs has a strong wavelength dependence and can even change sign (becoming repulsive) when the wavelength of the trapping light crosses the LSP resonance from the long-wavelength to the short-wavelength side of the resonance peak [REFS].

Optical trapping is a unique approach to address multiparticle assembly in liquid environment [Guffey & Scherer, NanoLett (2010)]. It requires neither lithographic patterning nor mechanical manipulation being a contactless technique. In Fig. 12 single MNPs are trapped in bulk solution and brought to contact with optically transparent substrates with for subwavelength positional accuracy. Finally optically trapped individual or aggregated [Messina *et al*. ACS Nano (2011)] MNPs can be used as efficient optical probes, for spectroscopy in liquid environment as demonstrated by recent experiments where surface-enhanced Raman spectroscopy (SERS) is obtained in an optical trap [Messina *et al*. J Phys Chem C (2011)].

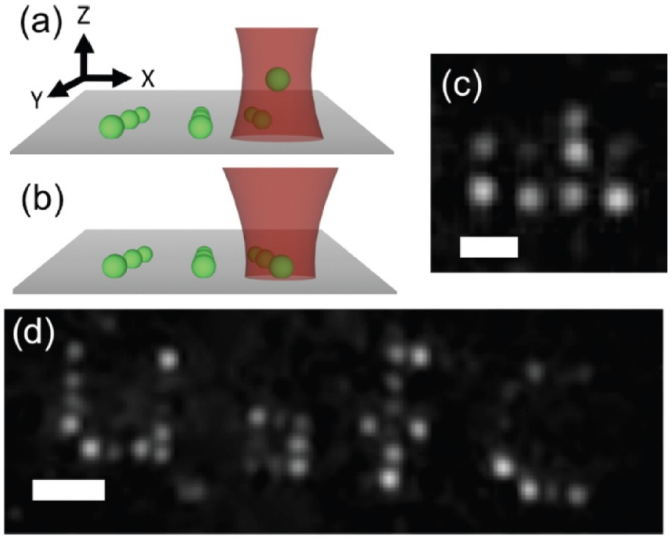

Figure 12. Schematic of single gold nanoparticle trapping (a) and deposition (b). (c) Dark-field image of typical pattern used for the determination of the precision of deposition (scale bar 2 μm). (d) "U of C" pattern created from 37 single nanoparticles (scale bar 4 μm). (Reprinted from [Guffey *et al*. (2010)]).

4.e. Low-dimensional nanostructures

Optical trapping has been recently extended to low-dimensional nanostructures. Semiconductor nanowires [REFS], single-wall carbon nanotubes (SWNTs) bundles [REFS], and graphene [REF], a one-atom thick two-dimensional material, are examples of nanostructures that are highly anisotropic in geometry and optical properties. This large anisotropy affects dramatically both the optical forces acting on such particles and the hydrodynamic mobility in the surrounding fluid. Linear nanostructures are also ideally suited as probes in next generation photonic force microscopy because of their intrinsic nanometric transverse size and micrometric axial length that ensure very stable trapping. In Fig. 13 some examples of optical manipulation and trapping of linear nanostructures are shown. GaN, SnO_2, ZnO or Si nanowires with different transverse size (20-200 nm range) and length (1-100 μm) were suspended in water and the suspension was transferred by means of a pipette into a chamber. Nanowires were stably trapped [REF] using near-infrared (NIR) light. Junctions and assemblies were then built using optical tweezers [REF]. Potassium niobate ($KNbO_3$) nanowires were also optically trapped [REF]. These wires exhibit efficient second harmonic generation, and act as frequency converters, allowing the

local synthesis of a wide range of colors via sum and difference frequency generation. Thus an optically trapped $KNbO_3$ can be used as a tunable nanometric light source to implement a novel form of subwavelength microscopy, in which an optical tweezers are used to trap and scan a nanowire over a sample, suggesting a wide range of potential applications.

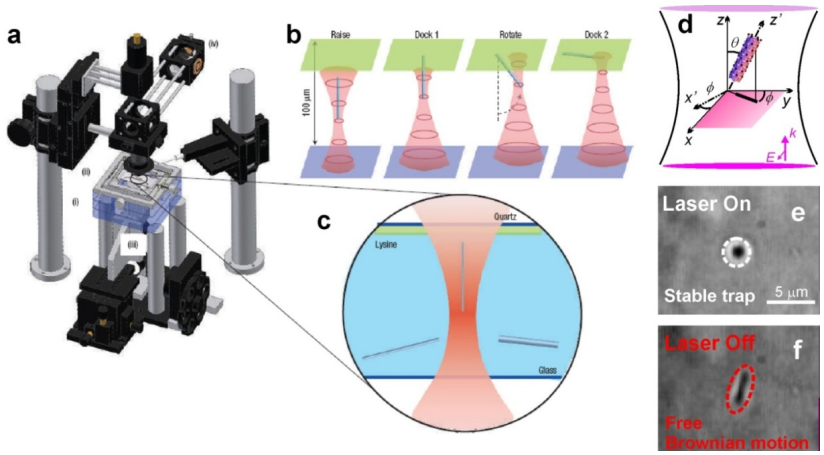

Figure 13. Optical trapping of linear nanostructures. (a) Setup for the trapping and manipulation of nanowires. (b) Schematic of the four-step nanowire positioning procedure. (c) Schematic of the experimental chamber cross-section. Owing to gravity, free nanowires sink to the bottom surface, where they can be picked up and assembled with the optical trap. (Reprinted from ref. …). (d) Optical trapping of carbon nanotubes. Geometry with Euler angles relevant in the optical trapping of nanotubes. (e) A laser trapped nanotube bundle oriented by radiation torque along the optical axis. (f) The same bundle un-trapped (laser is off) and randomly oriented by Brownian motion [(d,e,f) redrawn from Maragò *et al*., (2008)].

Carbon nanotube bundles [Maragò *et al*. (2008)] were also trapped using NIR light. Figures 12 (e,f) show a SWNT bundle when optically trapped (Fig. 13e) and aligned with the laser propagation direction (the imaging axis) and when untrapped (Fig. 13d) freely floating and randomly oriented. Graphene has been efficiently dispersed and optically trapped in water. Optical tweezers have been used to manipulate such graphene flakes and to study their Raman spectroscopy and Brownian dynamics in the trap [Maragò *et al*. (2010)]

When dealing with quantitative measurements and force calibration, anisotropy has a large influence on optical forces and torques, as well as particle hydrodynamics. *E.g.*, for exemplar linear nanostructures (rigid rod-like structures), the viscous drag is described by an anisotropic tensor [Happel (1981)], the components of which depend on the length-to-diameter ratio p=L/d as [Broersma (1981), Tirado]:

$$\gamma_{\perp} = \frac{4\pi\eta L}{\ln p + \delta_{\perp}}, \gamma_{\parallel} = \frac{2\pi\eta L}{\ln p + \delta_{\parallel}}, \gamma_{\Theta} = \frac{\pi\eta L^3}{3(\ln p + \delta_{\theta})} \qquad (4.e.1)$$

where $\gamma_{\perp}$ and $\gamma_{\parallel}$ are the translational mobilities, transverse and parallel to the main axis, γ_{Θ} is the rotational mobility about midpoint, η is the water dynamical viscosity, and δ_i are end corrections (calculated in [Broersma (1981), Tirado] as a polynomial of $(\ln 2p)^{-1}$) [see also Maragò *et al*. (2008)].

Nanotubes [Ref] and grapheme [REF] have been used as model anisotropic particle to extract the distribution of both centre-of-mass and angular fluctuations from three-dimensional tracking. The optical force and torque constants from auto and cross-correlation of the tracking signals were measured. The latter allowed the isolation of the angular Brownian motion, and hence a full calibration of the optical tweezers. In particular nanotubes and more generally linear nanostructures can consequently be used as force sensing probes in photonic force microscopy applications. For optically trapped low-dimensional nanostructures (nanowires, nanotube bundles, graphene flakes, *etc*.), positional and angular displacements from equilibrium are detected through

interferometric methods as for latex beads. While for spherical objects the detector signals are combined so that they are proportional to the centre-of-mass displacements, for non-spherical particles they also contain angular information. The projections onto the laboratory axes are determined through the relevant Euler angles (φ, θ) and the corresponding rotation matrix. Let us consider the case of a trapped linear nanostructure (see Fig. 13d). Since radiation pressure aligns the trapped linear structure with the light propagation axis, z, fluctuations occur in the small polar angle limit, $\theta << 1$, and the tracking signals are [Marago(2008), Jones(2009), Marago(2010)]:

$$S_x \propto X + a\Theta_x,\ S_y \propto Y + b\Theta_y,\ S_z \propto Z \qquad (4.e.2)$$

Where X, Y, and Z are the center-of-mass coordinates, a, b, c are calibration factors, and $\Theta_x = \theta\sin\varphi$ and $\Theta_y = \theta\cos\varphi$ are the projections on the x and y axis, respectively (shown in Fig. 13d).

The center-of-mass X_i and angular Θ_j coordinates are treated as stochastic variables. Thus, the Brownian dynamics of the trapped linear nanostructure can be described by a set of uncoupled Langevin equations:

$$\frac{d}{dt}X_i(t) = -\omega_i X_i(t) + \xi_i(t),\ i = x,y,z \qquad (4.e.3)$$

$$\frac{d}{dt}\Theta_j(t) = -\Omega_j \Theta_j(t) + \xi_j(t),\ j = x,y \qquad (4.e.4)$$

Where $\omega_i = k_i/\gamma_i$ and $\Omega_j = k_j/\gamma_\Theta$ are relaxation frequencies, related to the force and torque constants and viscous damping tensor components, while $\xi_i(t)$ are random noise sources. From Eqs 4.e.2, 4.e.3, and 4.e.4, the autocorrelations of the transverse tracking signals $C_{ii}(\tau) = \langle S_i(t)S_i(t+\tau)\rangle$ now contain combined information on center-of-mass and angular fluctuations, and decay with lag time τ as a double exponential with positional and angular relaxation frequencies ω_i, Ω_i (i=x, y). Furthermore, as the angular variables are geometrically correlated, the cross-correlations $C_{xy}(\tau) = \langle S_x(t)S_y(t+\tau)\rangle = C_{xy}(-\tau)$ of the transverse signals decay as single exponentials with relaxation rates corresponding to the angular degrees of freedom, Ω_x and Ω_y. This also allowed measurement of an optical torques of the order of 1pN•μm on the trapped nanotube bundle. Figure 9 (bottom plots) shows the temporal evolution of Brownian motion of a trapped nanotubes bundle with a transverse size of 10 nm and a length of 3 μm, to be compared with the one of a trapped 2-mm latex bead, top plots, as reconstructed through the tracking of the fluctuating tracking signals. Transverse displacements within 10 nm are measured, while the force calibration makes the trapped bundle a very sensitive probe of forces in the axial direction with resolution at the femto-newton [Maragò *et al*. (2008)]. These combined force and torque measurements enable the calibration of the optical tweezers when using linear nanostructures as force sensing probes in the femto-newton regime.

4.f. Optical trapping in vacuum

Thus far optical trapping of colloids has been discussed always in a liquid environment. We have seen that in this context the fluid viscosity is so strong that the motion of the particle in the trapping potential is over-damped. On the other hand OT can be achieved in vacuum, *i.e.*, in a chamber with a vacuum pressure so low that the ballistic regime and harmonic oscillations can now be observed [REFS]. Recently using a silica bead in a double optical tweezers in vacuum, ultra-high resolution measurements of its instantaneous velocity were performed [Li *et al*. (2010)]. These data directly verified the Maxwell-Boltzmann distribution and equipartition theorem for a Brownian particle (see Fig. 14) showing that for different pressure the velocity distribution of the bead is fitted by the same Maxwell-Boltzmann distribution.

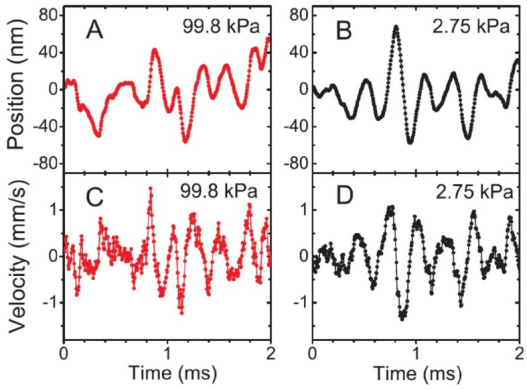

Figure 14. Position (A and B) and instantaneous velocity (C and D) of a 3-µm silica bead trapped in vacuum at two different background pressures. (Reprinted from ref. [Li *et al*. (2010)]).

This type of experiment has been the starting point for a controlled cooling of the centre-of-mass motion of a trapped particle. The scheme sketched in Fig. 15a, is based on the use of pairs of counter-propagating beams with independently controllable power in a similar fashion as what is typically used for laser cooling of atoms [C.J. Foot, Atomic Physics]. In this case a feedback can be adjusted on the beam power according to the velocity of the trapped particle so that the excess radiation pressure of one beam will counteract the motion of the bead. The result is an effective cooling that reaches temperatures in the millikelvin range (Fig. 15b). These achievements open perspectives toward the cooling of colloidal particles to the quantum ground motional state in vacuum [Papers by Cirac & Quidant].

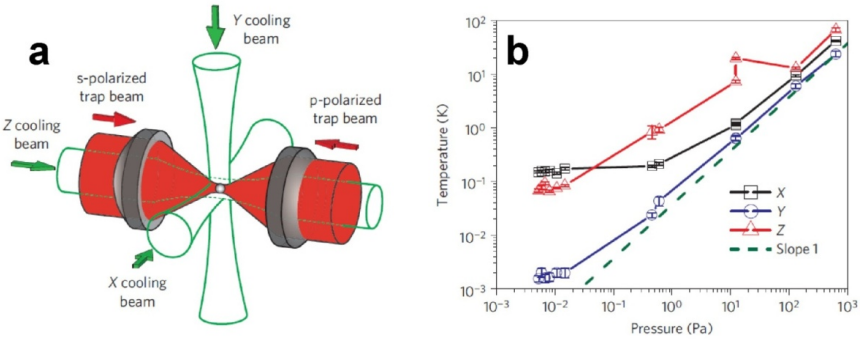

Figure 15. (a) Experimental setup for feedback cooling of a microparticle. A double optical tweezers (red beams) create a trapping potential where the particle is held. Six additional counter-propagating beams (green beams) generate the active feedback-cooling configuration. (b) Equilibrium temperature of a 3-µm silica bead laser cooled at different background pressures. Temperatures in the millikelvin range are achieved. (Reprinted from ref.…)

5. Many-particle systems and extended light fields: *The power of many.*

Large collections of colloidal particles have been manipulated using light fields. Such techniques have been particularly useful to study complex phenomena occurring in soft matter physics and in material physics.

5.a. Optical ratchets and sorting in optical lattices

GABE Ratchets: Roberto & the Reichhardts; Sorting: us (why? Less stress than centrifugation? – Greater selectivity?)

5.b. Optical crystallization and melting

… Fournier, Clemens Bechinger! (Highlight the corral!) Charles Reichhardt! Nucleation = Alfons van Blaaderen (Dirk Vossen)

5.c. Optical crystals and quasi-crystals

… Discuss David Nelson? Orientational order parameter; Adapt this section to include glass transition;

6. Advanced techniques: *One beam to rule them all.*

In recent years various more complex applications of optical forces have been proposed. These have come about either by engineering the properties of the light fields used in the optical manipulation or by applying standard optical manipulation techniques to new problems. In this section we review some of the most successful and promising ones.

6.a. Holographic optical tweezers

GABE Local phase control over the light waves used can provide for trap "steering" in 3D, for multiplexing the beam into multiple trap sites, or for tailored beam shaping.

The most basic form of beam shaping is aberration correction, which can be essential in complex optical systems, in order to preserve the strong gradients required for single-beam optical tweezers. High numerical-aperture (NA) objective lenses create strong gradients in the optical fields, giving both high *resolution* and *trapping strength*, but sensitivity to optical *aberrations* is *exponentially* worse for higher NA systems [Booth *et al.*, *J. Microsc.*, **192** (1998)]. Thus, trapping is quite sensitive to wavefront distortions. Aberration correction allows for maximal trapping strength while minimizing the laser power (in the specimen plane): this is key to minimizing undesirable effects due to the laser (*e.g.,* heating, or in the case of bacterial trapping, creation of excited oxygen states that can damage the living organism).

Recent work has demonstrated that aberration correction can yield an order of magnitude reduction in the required power, trapping at a small fraction of a milli-Watt [Cizmar *et al.*, *Nature Photonics* **XXX** (2010)]. Moreover, this same work demonstrated that it is possible to provide sufficient correction to trap through highly turbid media (so long as the time scales associated with scattering in the sample are long enough to be amenable with the correction algorithm employed). As a number of other approaches to wavefront correction do not allow compensation of distortions that occur within the sample itself, this is a significant advance.

Program a **Spatial Light Modulator** to implement a recent method[2] to correct for **optical *aberrations***

For every element added to the optical path there is some amount of insertion loss (*i.e.*, a reduction in the transmitted intensity). So, in part, the reduction in the number of optical elements was aimed at reducing the integrated insertion loss. Also of great significance, for our application, is the need to reduce the overall aberration present in the system. Our goals for the immediate future are to assess the effectiveness of (and trade-offs associated with) several independent techniques for aberration correction, including one of our own design.

We impose local phase shifts in the Fourier plane

Became popular with the publication of straightforward recipes [Dufresne, then Curtis, then deMarco], and implementation using Spatial Light Modulators [Curtis, a couple from Glasgow].

Note efficiency criteria vary (every pixel, uniformity, speed). – Note speed of GPU.

Overviews are available [

novel beam shapes light line, curved, bottle beam.

6.b. Beams with orbital angular momentum

GABE Note fN is one thing, but zN•m is really an unexplored domain of science! – Note Michelle Wang of Cornell.

6.c. Applications to microfluidics

The experimental generation and characterization of fluid flows in micro-environments is important both from a fundamental point of view and from an applied one, since for many applications it is required to assess the performance of microfluidic structures, such as lab-on-a-chip devices. Carrying out this kind of measurements can be extremely challenging. In particular, due to the small size of these environments, wall effects cannot be neglected. Additional difficulties arise studying biological fluids because of their complex rheological properties.

In the cases of practical interest the flow is strongly viscous (creeping motions or Stokes flows) and a low Reynolds number regime can be assumed. Since the creeping motion regime is a particular case of a laminar regime, it is possible to univocally define a time-independent pressure and velocity field. Therefore, for each position a well-defined drag force acts on a particle immersed in the fluid flow. Ideally micro-flow sensors should be able to monitor the streamlines in real time and in the least invasive way. One common method to achieve this goal is to measure the drag force field acting on a probe particle, resorting to statistical criteria of analysis because of the intrinsic presence of Brownian motion.

Recently optically trapped microscopic particles have been proposed as flow sensors. For example, an oscillating optically trapped probe is used to map the two-dimensional flow past a microscopic wedge [Nemet and Cronin Golomb (2002)]. A stress microviscometer was presented by Bishop *et al*. (2004) and by Knöner *et al*. (2005): it generates and measures microscopic fluid velocity fields, monitoring the probe particle displacement, which is directly converted into velocity field values, through digital video microscopy. A further improvement was achieved by using multiple holographic optical traps in order to parallelize the technique [Di Leonardo *et al*. (2006)]: an array of micro-probes can be simultaneously trapped and used to map out the streamlines in a microfluidic device. Finally, in a technique to characterize fluid flows above the first order was proposed, needed, *e.g.*, in the proximity of fixed points of the flow [Volpe *et al*. (2008)].

Add a final note on combining optical traps with other approaches (dielectrophoresis, magnetic tweezers, sonotweezers, etc.)

7. Bibliography

Ashkin, A. (1970). Acceleration and trapping of particles by radiation pressure. Phys. Rev. Lett. **24**, 156.

Ashkin, A., and Dziedzic, J.M. (1971). Optical levitation by radiation pressure. Appl. Phys. Lett. **19**, 283.

Ashkin, A., Dziedzic, J.M.,Bjorkholm, J.E., and Chu, S. (1986). Observation of a single-beam gradient optical trap for dielectric particles. Opt. Lett. **11**, 288.

Ashkin, A. (2000). History of Optical Trapping and Manipulation of Small-Neutral Particle, Atoms, and Molecules. IEEE J. Sel. Top. Quant. El. **6**, 841.

Berg-Sørensen, K., and Flyvbjerg, H. (2004). Power spectrum analysis for optical tweezers. Rev. Sci. Instrumen.**75**, 594.

Bishop, A.I.,Nieminen, T.A., Heckenberg, N.R., and Rubinsztein-Dunlop, H. (2004). Optical microrheology using rotating laser-trapped particles. Phys. Rev. Lett. **92**, 198104.

Broersma S. (1981) J. Chem. Phys. 74:6989.

Brown, R. (1828). A brief account of microscopical observations made in the months of June, July and August, 1827, on the particles contained in the pollen of plants; and on the general existence of active molecules in organic and inorganic bodies. Phil. Mag. **4**, 161.

Binnig, G., Quate, C.F., and Gerber, C. (1986). Atomic force microscope.Phys. Rev. Lett.**56**, 930.

Burns, M.M., Fournier, J.-M., and Golovchenko, J.A. (1989). Optical binding. Phys. Rev. Lett. **63**, 1233.

Di Leonardo, R., Leach, J., Mushfique, H., Cooper, J.M.,Ruocco, G., and Padgett, M.J. (2006). Multipoint holographic optical velocimetry in microfluidic systems. Phys. Rev. Lett. **96**, 134502.

Einstein, A. (1905).Über die von dermolekularkinetischenTheoriederWärmegeforderteBewegung von in ruhendenFlüssigkeitensuspendiertenTeilchen. Ann. Phys. **17**, 549.

Florin, E.-L., Pralle, A.,Stelzer, E.H.K., and Hörber, J. K. H. (1998). Photonic force microscope calibration by thermal noise analysis. Appl. Phys. A **66**, S75.

Foot C. J. (2005) *Atomic Physics*, Oxford University Press, Oxford, UK.

Ghislain, L.P., and Webb, W.W. (1993). Scanning-force microscope based on an optical trap. Opt. Lett. **18**, 1678.

Ghislain, L.P.,Switz, N.A., and Webb, W.W. (1994). Measurement of small forces using an optical trap. Rev. Sci. Instrumen. **69**, 2762.

Gouy, M. (1888). Note sur le mouvementbrownien. Journal de Physique, serie 2,**7**, 561.

Hajizadeh, F.; Reihani, S. N. S. Optimized Optical Trapping of Gold Nanoparticles. Opt. Exp. (2010), **18**, 551–559.

Hansen, P. M.; Bhatia, V. K.; Harrit, N.; Oddershede, L. Expanding the Optical Trapping Range of Gold Nanoparticles. Nano Lett. (2005), **5**, 1937–1942.

Happel J & Brenner H. (1981) *Low Reynolds Number Hydrodynamics*. Springer, Berlin.

Henderson S, Mitchell S, Bartlett P. (2001) Position correlation microscopy: probing single particle dynamics in colloidal suspensions. Colloids and Surfaces A **190**, 81-88.

Huang, R., Chavez, I., Taute,K.M.,Lukić, B.,Jeney, S., Raizen, M.G., and Florin, E.-L. (2011). Direct observation of the full transition from ballistic to diffusive Brownian motion in a liquid. Nat. Phys. doi:10.1038/nphys1953

Knöner, G., Parkin, S., Heckenberg, N.R.,and Rubinsztein-Dunlop, H. (2005). Characterization of optically driven fluid stress fields with optical tweezers. Phys. Rev. E **72**, 031507.

Langevin, P. (1908). Sur la theórie du mouvementbrownien. C. R. Acad. Sci. (Paris) **146**,530.

Li, T., Kheifets, S., Medellin, D., andRaizen, M. G. (2010).Measurement of the instantaneous velocity of a Brownian particle.Science 328, 1673.

Martin, S.; Reichert, M.; Stark, H.; Gisler, T. Direct Observation of Hydrodynamic Rotation-Translation Coupling between Two Colloidal Spheres. Phys. Rev. Lett. (2006), **97**, 248301.

Meiners J-C and Quake SR. (1999) A Direct Measurement of Hydrodynamic Cross Correlations Between Two Particles in an External Potential. Phys. Rev. Lett. **82**, 2211.

Nelson, E. (1967). Dynamical Theories of Brownian Motion (Princeton University Press).

Nemet, B.A., and Cronin-Golomb, M. (2002). Microscopic flow measurements with optically trapped microprobes. Opt. Lett.**27**, 1357.

Saija, R.; Denti, P.; Borghese, F.; Maragò, O. M.; Iatì, M. A. Optical Trapping Calculations for Metal Nanoparticles. Comparison with Experimental Data for Au and Ag Spheres. Opt. Exp. (2009), **17**, 10231–10241.

Seol, Y; Carpenter, A. E.; Perkins, T. T. Gold Nanoparticles: Enhanced Optical Trapping and Sensitivity Coupled with Significant Heating. Opt. Lett. (2006), **31**, 2429–2431.

Svoboda, K.; Block, S. M. Optical Trapping of Metallic Rayleigh Particles. Opt. Lett. (1998), **28**, 930–932.

Pecseli, H. L. (2000). *Fluctuations in Physical Systems.* Cambridge University Press, Cambridge, UK

Pralle A, Prummer M, Florin E-L, Stelzer EHK, Hörber JKH. (1999). Three-dimensional high-resolution particle tracking for optical tweezers by forward scattered light. Microsc. Res. Tech. **44**, 378–386.

Rohrbach A (2005) Stiffness of Optical Traps: Quantitative Agreement between Experiment and Electromagnetic Theory. Phys. Rev. Lett. **95**, 168102.

Tatarkova, S.A.,Carruthers, A.E., and Dholakia, K. (2002). One-Dimensional Optically Bound Arrays of Microscopic Particles. Phys. Rev. Lett. **89**, 283901.

Uhlenbeck, G.E., and Ornstein, L.S. (1930). On the theory of Brownian Motion. Phys. Rev. **36**, 823.

Volpe, G., Volpe, G.,and Petrov, D. (2008). Singular point characterization in microscopic flows. Phys. Rev. E **77**, 037301.

Volpe, G., Wehr, J., Petrov, D., and Rubi, J.M. (2009). Thermal noise suppression: How much does it cost? J. Phys. A: Math. Theor. **42**, 095005.

[see *e.g.*, Arias-Gonzalez&Nieto-Vesperinas, JOSA A 2003, 20, 1201; Pelton *et al*., Opt. Lett. 2006, 31, 2429; Toussaint *et al*., Opt.Express 2007, 15, 12017; Gaugiran *et al*., Opt.Express 2007, 15, 8146; Dienerowitz *et al*., Opt.Express 2008, 16,4991; Guffey&Scherer, NanoLett.2010; Jones *et al*., ACS Nano 2009, 3, 3077; Saija *et al*., Opt.Express, 2009, 17, 10231; Messina *et al*., ACS Nano (2011); Messina *et al*. J Phys Chem C (2011)].